Chronological constraints on the Paleoproterozoic Francevillian Group in Gabon

AUTHOR(S):

Sawaki, Yusuke; Moussavou, Mathieu; Sato, Tomohiko; Suzuki, Kazue; Ligna, Cédric; Asanuma, Hisashi; Sakata, Shuhei; Obayashi, Hideyuki; Hirata, Takafumi; Edou-Minko, Amboise

CITATION:

Sawaki, Yusuke ...[et al]. Chronological constraints on the Paleoproterozoic Francevillian Group in Gabon. Geoscience Frontiers 2017, 8(2): 397-407

ISSUE DATE:

2017-03

URL:

http://hdl.handle.net/2433/227738

Geoscience Frontiers 8 (2017) 397–407

HOSTED BY

ELSEVIER

Contents lists available at ScienceDirect

China University of Geosciences (Beijing)

Geoscience Frontiers

journal homepage: www.elsevier.com/locate/gsf

Research paper

Chronological constraints on the Paleoproterozoic Francevillian Group in Gabon

Yusuke Sawaki [a,*], Mathieu Moussavou [b], Tomohiko Sato [c], Kazue Suzuki [a], Cédric Ligna [b], Hisashi Asanuma [a], Shuhei Sakata [d], Hideyuki Obayashi [e], Takafumi Hirata [f], Amboise Edou-Minko [b]

[a] Department of Earth and Planetary Sciences, Tokyo Institute of Technology, 2-12-1 O-okayama, Meguro-ku, Tokyo 152-8551, Japan
[b] University of Sciences and Technology in Masuku, BP:901, 90025 Franceville, Gabon
[c] Earth-Life Science Institute (ELSI), Tokyo Institute of Technology, 2-12-1 O-okayama, Meguro-ku, Tokyo 152-8551, Japan
[d] Department of Chemistry, Gakushuin University, Mejiro 1-5-1, Toshima-ku, Tokyo 171-8588, Japan
[e] Division of Earth and Planetary Sciences, Graduate School of Science, Kyoto University, Kitashirakawa Oiwake-cho, Sakyo-ku, Kyoto 606-8502, Japan
[f] Geochemistry Research Center, The University of Tokyo, Hongo 7-3-1, Bunkyo-ku, Tokyo 113-0033, Japan

ARTICLE INFO

Article history:
Received 31 March 2016
Received in revised form
16 September 2016
Accepted 3 October 2016
Available online 8 October 2016

Keywords:
Gabon
Francevillian Group
Paleoproterozoic
N'goutou complex
Zircon
MC-ICP-MS

ABSTRACT

The Francevillian Group in Gabonese Republic was recently established as a typical sedimentary sequence for the Paleoproterozoic. However, its age is rather poorly constrained, mainly based on Rb-Sr and Nd-Sm datings. This study reports new zircon data obtained from Chaillu massif and N'goutou complex, which constrain the protolith age of the basement orthogneisses and the igneous age of an intrusive granite, respectively. Most zircons from the orthogneisses are blue and exhibit oscillatory zoning in cathode-luminescence images. Zircons with lower common lead abundances tend to be distributed close to the concordia curve. Two age clusters around 2860 Ma and 2910 Ma are found in zircons plotted on the concordia curve. Based on the Th/U ratios of zircons, these ages correspond to the protolith ages of the orthogneisses, and the zircons are not metamorphic in origin. Syenites and granites were collected from the N'goutou complex that intrudes into the FA and FB units of the Francevillian Group. The granitoids exhibit chemical composition of A-type granite affinity. Half of zircons separated from the granite are non-luminous, and the remaining half exhibit obscure internal textures under cathode-luminescence observation. All zircon grains contain significant amounts of common lead; the lead isotopic variability is probably attributed to the mixing of two components in the zircons. The zircon radiogenic $^{207}Pb/^{206}Pb$ ratio is 0.13707 ± 0.0010, corresponding to a $^{207}Pb/^{206}Pb$ age of 2191 ± 13 Ma. This constrains the minimum depositional age of the FA and FB units. Furthermore, the FB unit consists of manganese-rich carbonate rocks and organic carbon-rich black shales with macroscopic fossils. Based on our age constraints, these organisms appeared in the study area just after the last Paleoproterozoic Snowball Earth event, in concert with global scale oxidation event encompassing the Snowball Earth.

1. Introduction

The Paleoproterozoic is one of the most important periods through Earth's history and is characterized by numerous geological events such as the emergence of eukaryotes (e.g., Han and Runnegar, 1992), Snowball Earth events (e.g., Kopp et al., 2005), and the oxygen level increase in the ocean-atmosphere system (e.g., Rye and Holland, 1998; Holland, 1999, 2005). Recently, macroscopic structures, which can be interpreted as colonial organisms and microbial/algal consortia, were reported from Paleoproterozoic sedimentary rocks (Francevillian Group) in Gabonese Republic (Albani et al., 2010; Moussavou et al., 2015). Several geochemical proxies were measured in the sediments in order to decipher the surface paleoenvironmental conditions at that time (Gauthier-Lafaye and Weber, 2003; Préat et al., 2011; Canfield et al.,

* Corresponding author. Fax: +81 3 5734 3538.
E-mail addresses: y-sawaki@geo.titech.ac.jp (Y. Sawaki), edouminko@gmail.com (A. Edou-Minko).
Peer-review under responsibility of China University of Geosciences (Beijing).

http://dx.doi.org/10.1016/j.gsf.2016.10.001

2013). The Francevillian Group, in particular, attracted significant attention from many scientific fields, because it contains the well-known Oklo natural reactors (Neuilly et al., 1972; Gauthier-Lafaye et al., 1989) and excellent manganese-rich carbonate rocks (Weber, 1968) in the FA and FB unit. Nevertheless, the chronological constraints on the sedimentary sequences are still insufficient. Especially, the maximum and minimum depositional ages of sediments containing the above macroscopic structures and natural reactors have been only poorly constrained by the ages of the basement rocks and intrusive granitoids (Bonhomme et al., 1982; Caen-Vachette et al., 1988; Moussavou and Edou-Minko, 2006). Here, we report new precise protolith zircon ages of the basement gneiss and the igneous age of the intrusive granite in the N'goutou complex. These more precise documentations will allow correlating the Francevillian Group with sedimentary sequences in other areas, which is important to understand the order of events occurring in the Paleoproterozoic.

The basement beneath the Francevillian Group is mainly composed of granitoids including granite, monzonite, syenite, diorite, and gneiss. The extensive work by Caen-Vachette et al. (1988) has considerably enhanced our knowledge of the geological history of these basement rocks. Based on the Rb-Sr isochron method and U-Pb isotope systematics, they suggested the following phases: (1) 3000–2850 Ma; high-grade metamorphism in the eastern Makokou area and formation of the Chaillu gneisses; (2) 2850–2700 Ma; high-grade metamorphism of the western Makokou gneisses and the main magmatic phase in the Chaillu area; (3) 2700–2600 Ma; epizonal metamorphism and later magmatism in the Chaillu area. The data from all zircon grains, however, were plotted far from the concordia curve. Therefore, the ages for the individual granitoids, based on the discordia lines, are still rather uncertain. Moreover, this previous work did not include descriptions of the internal zircon structures obtained through cathode-luminescence (CL) observations and consideration for common Pb.

Plutonic rocks of the N'goutou complex intrude into the Paleoproterozoic Francevillian Group. Therefore, determining its intrusive age is important to constrain the minimum sedimentary age of the Francevillian Group. The age of the N'goutou complex was estimated through Rb-Sr (Bonhomme et al., 1982) and U-Pb datings (Moussavou and Edou-Minko, 2006) of syenites and pegmatite. The former gave an isochron age of 2143 ± 143 Ma, but a possibility of mixing (erroneous isochron) was not well discussed in this previous work. In addition, initial $^{87}Sr/^{86}Sr$ ratio of 0.7006 calculated from the isochron is too low for the 2.1 Ga in view of the secular evolution in the mantle $^{87}Sr/^{86}Sr$ ratio. On the other hand, Moussavou and Edou-Minko (2006) provided an upper intercept age of 2027 ± 55 Ma based on discordant zircon U-Pb data. Some zircon grains included a certain level of common Pb ($^{204}Pb/^{206}Pb > 0.0002$), and internal structures in zircon were not checked by conventional CL image.

In the present study, we collected basement orthogneisses of Chaillu massif from pluri-metric blocks enclosed in the FA units, northwest of Francevillian basin (GPS position: S1°43′14.4″, E13°18′24.5″), and an intrusive syenite and granite from the N'goutou complex in order to acquire chronological data that are more precise (Fig. 1). Our *in situ* U-Pb isotopic data were obtained through multi-collector, inductively coupled plasma mass spectrometry (MC-ICP-MS). The age data are discussed here together with CL observations and an evaluation of the common Pb abundance.

2. Geological background

2.1. Geological setting and isotopic history

Paleoproterozoic sedimentary sequences, named the Francevillian Group, are widespread in eastern Gabon Republic and rest unconformably on an Archean basement referred to as the East Gabonian block (Fig. 1a). The basement rocks are mainly composed of Mesoarchean granitoids and greenstone (Bonhomme et al., 1982; Caen-Vachette et al., 1988; Thiéblemont et al., 2014). Granitoids near Koulamoutou and Chaillu are dated at 2888 ± 40 Ma, 2765 ± 39 Ma, and 2637 ± 33 Ma based on Rb-Sr isochron (Fig. 1a; Caen-Vachette et al., 1988). The Paleoproterozoic Ogooué orogenic belt is located west of the Francevillian Group.

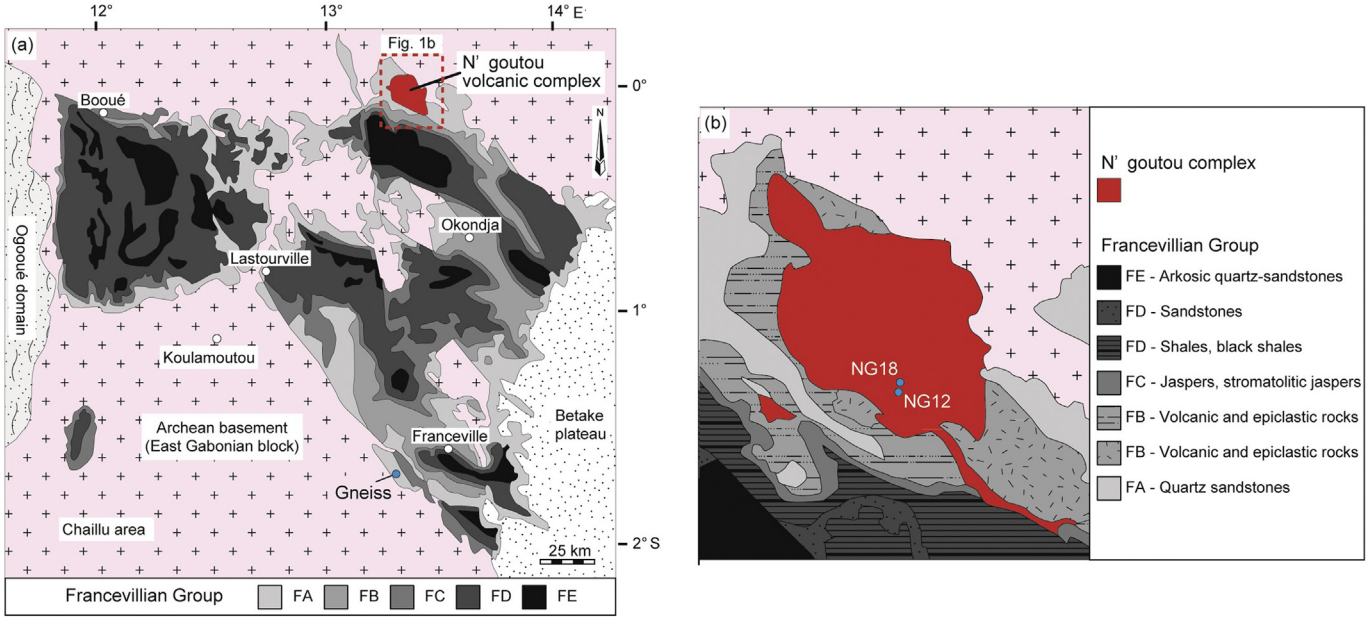

Figure 1. (a) Geological map of SE Gabon, including the distribution of the Francevillian Group (modified after Thiéblemont et al., 2014). (b) Simplified geological map around the N'goutou complex, showing the locations of granite and syenite (NG12 and NG18).

The tectono-thermal overprint in the Francevillian basin tends to attenuate eastward, and the Francevillian and Okondja sub-basins were less affected by metamorphism and deformation. The Francevillian Group is subdivided into five formations; named FA to FE from bottom to top, respectively (Weber, 1968). The basal FA unit is mainly composed of clastic sedimentary rocks. The depositional environment is considered as fluvial in the lower part and marine in the upper part (Gauthier-Lafaye and Weber, 2003). The FA unit is characterized by the occurrence of uranium deposits (e.g., Neuilly et al., 1972; Gauthier-Lafaye, 2006), which were dated at 2050 ± 30 Ma through the classical U-Pb methods on uraninites (Gancarz, 1978). The date of the fission reactions was determined by comparing the fluence of the fission reaction to the amount of fission elements produced, which provided an age of 1950 ± 30 Ma (Ruffenach, 1978; Holliger, 1988; Naudet, 1991). Oil-bearing fluid inclusion in quartz grains (within C1 layer) yielded hydrocarbon, including hopanes, 2α-methylhopanes, terpanes, and steranes (Dutkiewicz et al., 2007); poly aromatic hydrocarbon species were discovered in solid bitumen around Oklo natural fission reactors (Nagy, 1993; Nagy et al., 1993). The FB unit consists largely of shales and black shales with subordinate manganese-rich carbonate rocks and coarse-grained clastic rocks. Macroscopic structures, interpreted as colonial organisms (Albani et al., 2010), and complex ductile nodules, interpreted as microbial/algal consortia (Moussavou et al., 2015), have been reported from the upper FB unit. In addition, hydrocarbon species, such as alkanes and alkyl benzene, and organic matter of cyanobacterial affinity have been reported from the same unit (Nagy, 1993; Nagy et al., 1993; Amard and Bertrand-Sarfati, 1997). Diagenetic illites in the middle of the FB unit provide a Sm-Nd age of 2099 ± 115 Ma (Bros et al., 1992). The FC unit includes shallow marine dolostones and thin-banded cherts with stromatolite structures. The FD unit consists of black shales with ignimbrite tuff at the top. The youngest zircon U-Pb age from the tuff is 2083 ± 6 Ma (Horie et al., 2005), which constrains the maximum depositional age of the FD unit. The FE unit comprises epiclastic sandstones and intercalating shales.

In the northern part of the Okondja basin, the Francevillian rifting was accompanied by the emplacement of the N'goutou complex (Fig. 1). The N'goutou complex is a subvolcanic ring complex, which includes three successive intrusive units (Moussavou and Edou-Minko, 2006): (1) an external unit (N1) including syenites and microsyenites in the north and alkaline granite in the south; (2) an internal unit (N2) consisting of microgranites; and (3) a later internal unit (N3) made of porphyritic to pegmatitic syenites. These rocks exhibit an alkaline within-plate signature (Moussavou and Edou-Minko, 2006). Recently, Thiéblemont et al. (2014) identified N'goutou complex intrusions into the FA and FB units, which are overlain by the sediments of the FC unit (Fig. 1b).

To constrain the protolith age of the basement rocks, we collected orthogneiss samples (Gneiss) from the East Gabonian block at the northwest of Franceville basin (Fig. 1a).

2.2. Granitoid petrology

Rock samples for age determination were collected from the N1 unit of the N'goutou complex (Fig. 1b; GPS positions: S0°1′59.3″, E13°24′2.5″ (NG12) and S0°1′46.5″, E13°24′11″ (NG18)). The potassium-rich granite (NG12) and alkaline syenites (NG18) are mainly composed of medium- to coarse-grained K-feldspar and display equigranular textures (Fig. 2). The NG18 sample consists of aegirine, together with local quartz and ilmenite, and accessory fluorite and siderite (Fig. 2a–f). The NG12 sample consists of aggregated quartz crystals and illite (Fig. 2g, h) together with rutile and bastnäsite (Fig. 2i–l). These mineral assemblages are largely consistent with those reported by Moussavou and Edou-Minko (2006). Elemental maps, acquired using a Hitachi S-3400N scanning electron microscope (SEM; Hitachi High Tech. Corp., Japan) with a an X-ray energy dispersive spectroscope (EDS; Bruker Corp., USA), show that F is rich in some minerals such as aegirine, fluorite, and bastnäsite (Fig. 2d, j).

3. Sample preparation and analytical methods

3.1. Whole-rock compositions

The granite and syenite samples were prepared for whole rock chemistry. Thin (1–2 cm thick) rock chips weighing about 20 g were cut from fresh parts of the samples. Visible veins were avoided during this process. The chips were washed with distilled water using an ultrasonic device and dried completely at 120 °C overnight. Rock powders were prepared using a tungsten-carbide mill and an agate-ball mill. Then, they were dried at 110 °C and 950 °C (over 6 h), respectively.

Major element compositions (Si, Ti, Al, Fe, Mn, Mg, Ca, Na, K, and P) were determined with an X-ray fluorescence spectrometer (XRF; RIX 2100, RIGAKU) at the Tokyo Institute of Technology, Japan. Fused glass discs were prepared with a lithium tetraborate ($Li_2B_4O_7$) flux in a 1:10 dilution ratio at 1050 °C. During the XRF analysis, the accelerating voltage was 50 kV and the current was 50 mA. Calibration methods using GSJ standards were based on Machida et al. (2008). Repeated analyses of the same standard indicated that the reproducibility of this analysis was better than 1%, except for Na and P (<5%).

3.2. Zircons and their cathodoluminescence images

Zircons were extracted from the orthogneiss (Gneiss) and granite (NG12) using a standard mineral separation system at the Tokyo Institute of Technology. Most zircons from the orthogneiss are sub-euhedral and generally over 30 μm × 100 μm. From the granite, we picked up only shattered fractions of zircon; therefore, the original shapes of zircons are unclear.

The zircon grains were mounted in Epofix resin and polished until their midsections were exposed. The zircons' internal structure was analyzed using an SEM (Hitachi High Tech. Corp., Japan) with a Chroma CL2 sensor (Gatan, Inc., USA) and a an X-ray EDS (Bruker Corp., USA) at the Tokyo Institute of Technology. Most zircons from the orthogneiss were blue and exhibited zoning from the core to rim in the CL images (Fig. 3a). On the other hand, metamictization occurred in some zircons, which is evident in the elemental maps (Fig. 3c). The metamictized part was rich in Ca and Al and poor in Zr and Si, and appeared dark in the CL images. The alternating metamictized and non-metamictized parts were partially responsible for the observed zoning in the zircon CL images. About half of the zircons separated from the granite were non-luminous under CL observation. The remaining half exhibited obscure internal textures, some of which showed striped patterns in the CL images (Fig. 3b).

3.3. LA-ICP-MS analytical methods

In situ U-Pb dating was carried out on zircon using a Nu PlasmaII (Nu instruments, Wrexham, U.K.) MC-ICP-MS coupled to an NWR-193 laser-ablation system (ESI, Portland, USA) at Kyoto University, in a similar system previously described (Sakata et al., 2014; Higashino et al., 2015). Before spot analyses, the metamictized parts in the individual zircon grains were checked by weak pre-ablation, because such parts are easily broken compared to the parts that are unaffected by metamictization. We avoided analyzing

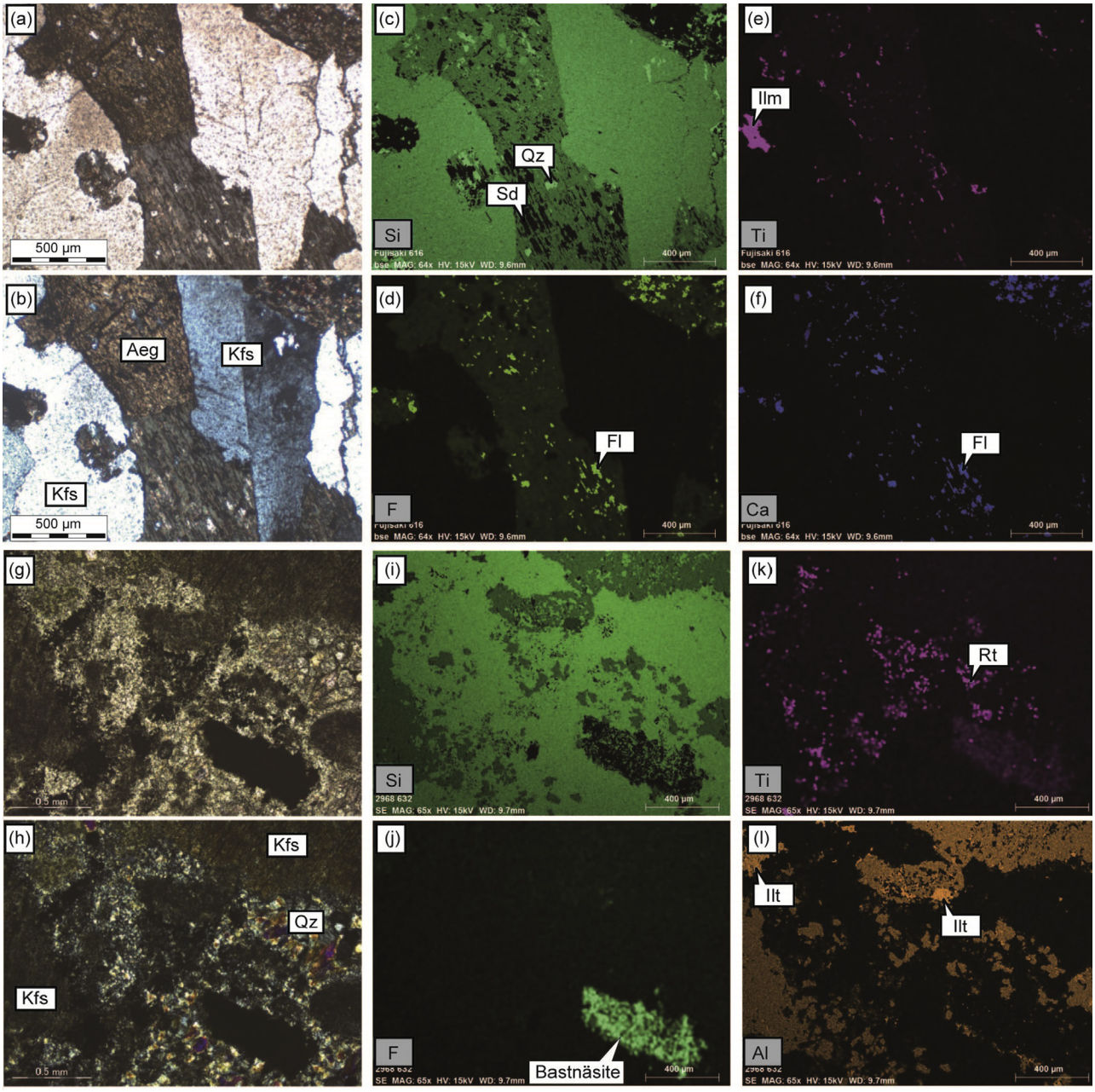

Figure 2. Microphotographs in plane and cross-polarized light and elemental maps obtained with SEM-EDS for syenite (a–f; NG18) and potassium-rich granite (g–l; NG12). Qz: quartz; Sd: siderite; Kfs: potassium feldspar; Ilm: ilumenite; Aeg: aegirine; Fl: fluorite; Rt: rutile; Ilt: illite.

such metamictized parts and mineral inclusions throughout the analyses. The diameter of the laser ablation spot was 20 μm. Helium gas was used as a carrier gas, promoting sample transport efficiency from the sample cell to the ICP and minimizing the re-deposition of the sample aerosol around the ablation pit (Eggins et al., 1998; Günther and Heinrich, 1999; Jackson et al., 2004). The plasma conditions and torch position were optimized to maximize signal intensities for ^{206}Pb, ^{207}Pb, and ^{235}U, while the thorium oxide ($^{232}Th^{16}O^{+}/^{232}Th^{+}$) formation rate was less than 0.5%. The detailed analytical conditions are shown in Table 1. In this study, the raw signal was monitored in the time-resolved analysis (TRA) mode, in order to avoid the contribution of non-radiogenic Pb from secondary inclusions or potential contamination of the analyzed area. The data acquisitions were based on the integration of the total ion counts per signal ablation. The integration length of a single ablation pit was 20 s. The same timing of integration windows was used for all unknown and standard samples, and the correction for downhole fractionation was not performed. The sample-standard bracketing technique was adopted to improve the reproducibility of the measurements. Analytical uncertainties were combined with counting statistics of signal intensities for monitored isotopes and their gas blanks, and the reproducibility of the standard analyses (NIST SRM612 and Nancy 91500) was added in quadrature. We used GJ-1 and Plešovice zircon grains as secondary standards, and monitored their U and Pb isotopic ratios. The results of the secondary standards were fitted to previously reported values (Jackson et al., 2004; Sláma et al., 2008) within the analytical errors throughout the analysis (Table 1). To evaluate the contribution of non-radiogenic Pb originating from inclusions or surface contamination, we monitored ^{204}Pb and ^{202}Hg throughout the analyses.

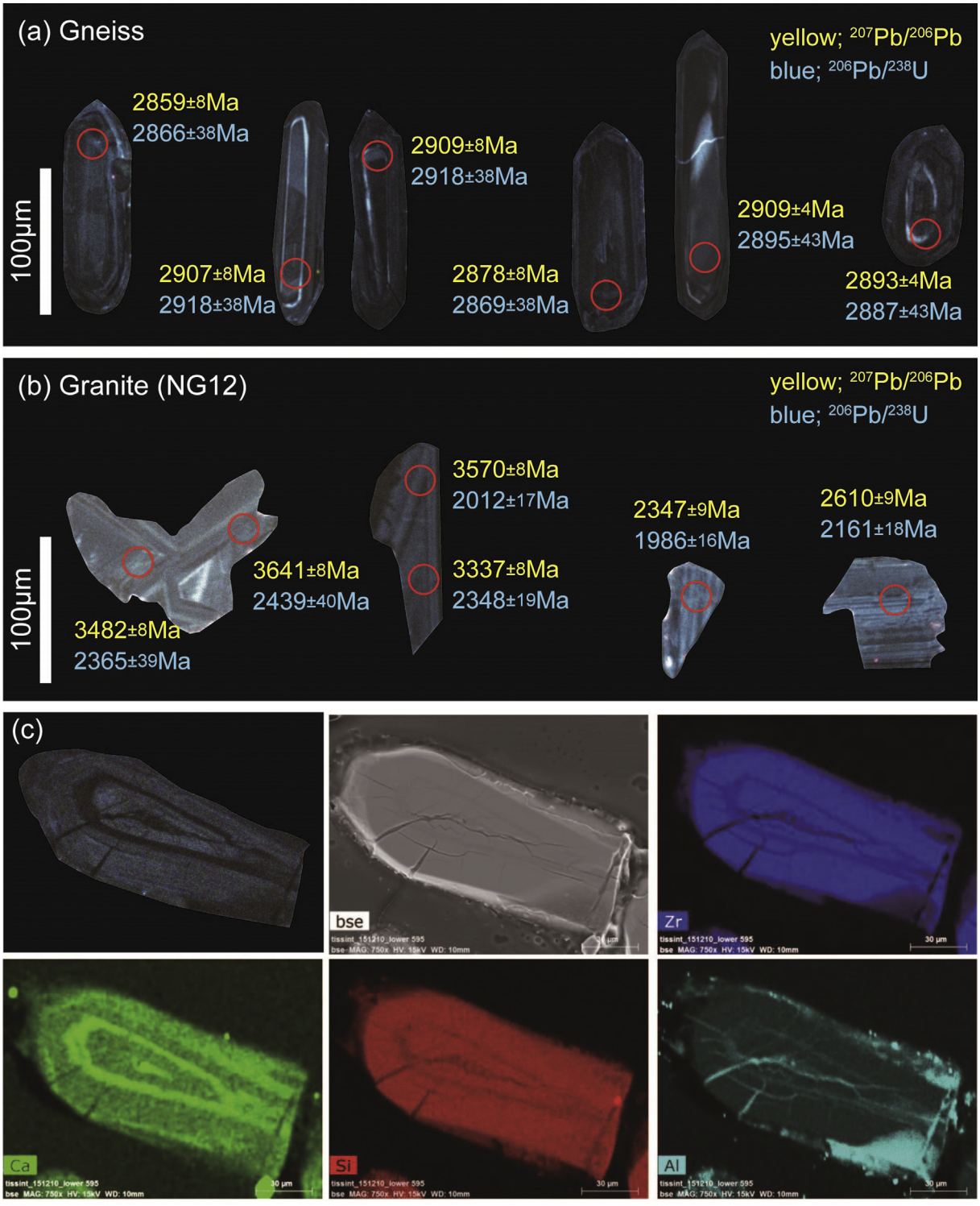

Figure 3. CL images of representative zircons from (a) an orthogneiss (Gneiss) and (b) a granite (NG12). Red circles mark analytical spots. $^{238}U/^{206}Pb$ and $^{207}Pb/^{206}Pb$ ages are expressed as yellow and blue characters, respectively. (c) CL image together with elemental maps of a locally metamictized zircon.

The signal intensity of ^{204}Pb was calculated by removing the contribution of the isobaric interference from ^{204}Hg, assuming the $^{204}Hg/^{202}Hg$ in zircon grains was the same as that in the gas blank. Common Pb correction was not made for the U-Pb ratios reported in Table 3. Tera-Wasserburg Concordia diagrams of all the zircons are illustrated in Fig. 4 using the ISOPLOT program of Ludwig (2003).

4. Results

4.1. Whole-rock chemical composition

The granitoids consist of 61.04 and 76.52 wt.% SiO_2 and 13.47 and 12.64 wt.% Al_2O_3 (Fig. 2). These samples are enriched in Na_2O and K_2O and depleted in MgO. Their high alkaline metal contents

Table 1
Instrumentation and operational settings.

Laser ablation system	
Instrument	NWR193 excimer laser (ESI, Portland, USA)
Cell type	Two volume cell
Laser wave length	193 nm
Pulse duration	<5 ns
Fluence	2.0–3.0 J/cm^2
Repetition rate	3–5 Hz
Ablation pit size	20 μm
Sampling mode	Single hole drilling
Pre-cleaning	1 shot with 50 μm
Carrier gas	He gas and Ar make-up gas combined outside ablation cell
He gas flow rate	0.60 L/min
Ar make-up gas flow rate	0.86–0.94 L/min
Ablation duration	30 s
Signal smoothing device	Enabled (Tunheng and Hirata, 2004)
ICP mass spectrometer	
Instrument	Nu PlasmaII HR-MC-ICP-MS (Nu Instruments, Wrexham, U.K.)
RF power	1300 W
Data reduction	Integration of total ion counts per single ablation. Signals obtained from first few seconds were not used for data reduction, and next signals obtained from 20 s were integrated for further calculations. Intensity of ^{238}U is calculated assuming ^{238}U/^{235}U = 137.88 (Jaffey et al., 1971).
Detection mode	Multiple collector mode
Detector	Four full size secondary electron multipliers (IC0, IC3, IC4 and IC5), two daly cups (D1 and D2) and 1 F cup (H9) were used.
Dead time	IC0: 15.8 ns, IC3: 14.7 ns, IC4: 18.9 ns, IC5: 20.0 ns, D1: 15.0 ns, D2: 8.6 ns
Monitored isotopes	^{202}Hg, ^{204}(Hg + Pb), ^{206}Pb, ^{207}Pb, ^{208}Pb, ^{232}Th, ^{235}U
Integration time per peak	20 s
Total integration time per reading	0.4 s
Formation rate of ^{232}Th^{16}O	0.40%
Data processing	
Gas blank	Gas blank counts were obtained for 20 s before each ablation pit.
Calibration strategy	91500 zircon was used in correction for Pb/U, Th/U fractionation and difference of detector's gain in all measurements. NIST SRM612 was used for correction of Pb/Pb mass bias and difference of detector's gain as well. GJ-1 (^{238}U-^{206}Pb age: 600.39 ± 0.65 Ma, ^{207}Pb-^{206}Pb age: 608.62 ± 0.36 Ma, Jackson et al., 2004) and Plešovice (337.13 ± 0.37 Ma, Sláma et al., 2008) were used as secondary standards for quality control.
Normalization values	^{206}Pb/^{238}U = 0.1793, U concentration = 81.2 μg/g, Th concentration = 28.6 μg/g, Pb concentration = 14.8 μg/g (91500, Wiedenbeck et al., 1995), ^{207}Pb/^{206}Pb = 0.90726, ^{206}Pb/^{204}Pb = 17.093, ^{207}Pb/^{204}Pb = 15.509, ^{208}Pb/^{204}Pb = 36.999 for NIST SRM612 (Jochum and Brueckner, 2008).
Common-Pb correction	Not made
Uncertainties	Uncertainties for ages and isotope ratios are quoted at 2 SD absolute, propagation is by quadratic addition. Reproducibilities of primary standard and counting statistics of measured isotopes and background counts are propagated.
Quality control/validation	GJ-1: weighted ave. ^{206}Pb/^{238}U age = 595.2 ± 8.5 Ma (2 SE, MSWD = 4.4, n = 7), ^{207}Pb/^{235}U age = 600.6 ± 7.0 Ma (2 SE, MSWD = 3.9, n = 7), ^{207}Pb/^{206}Pb age = 617.2 ± 3.9 Ma (2 SE, MSWD = 1.0, n = 7). Plešovice: weighted ave. ^{206}Pb/^{238}U age = 336.1 ± 3.9 Ma (2 SE, MSWD = 2.2, n = 6), ^{207}Pb/^{235}U age = 339.0 ± 2.8 Ma (2 SE, MSWD = 1.2, n = 6).

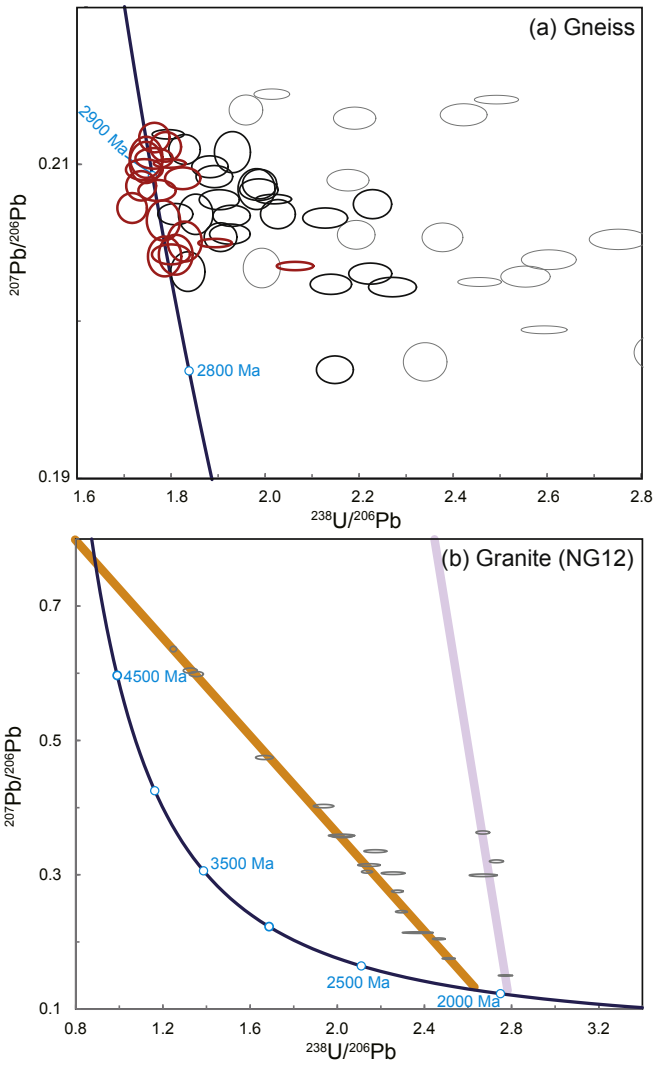

Figure 4. Tera-Wasserburg concordia diagrams of *in situ* U-Pb ages of zircons with LA-ICP-MS for (a) orthogneiss (Gneiss) and (b) a granite (NG12). These figures were constructed with an ISOPLOT (Ludwig, 2003). The error ellipses on the individual spots are at the 2σ level. Red circles represent zircons with few ^{204}Pb. Zircons with ^{204}Pb/^{206}Pb ratios over 0.0001 and 0.0005 are shown as black and gray circles, respectively.

and high K_2O/Na_2O ratios are consistent with the petrologic description (K-feldspar-rich mineral assemblage) and those reported from Moussavou and Edou-Minko (2006). Also considering the fact that F-bearing minerals are rich, these granitoids have chemical compositions of A-type granite affinity. The high SiO_2 content (76.52 wt.% SiO_2) and the high aluminum saturation index (1.20) of NG12 reflect a certain amount of quartz and the existence of illite, respectively (Fig. 2g, h). On the other hand, the Fe-rich chemical composition (10.48 wt.% Fe_2O_3) and the low aluminum saturation index (0.82) of NG18 are consistent with the occurrence of aegirine.

4.2. Orthogneiss zircon U-Pb ages

The ^{207}Pb/^{206}Pb ages of zircons from the orthogneiss (Gneiss) range from *ca.* 2483 to 3311 Ma (Table 3). About 20% of the zircons are plotted on the Tera-Wasserburg concordia curve within an analytical error (Fig. 4a). About 70% of zircons contain certain amounts of common lead (^{204}Pb/^{206}Pb > 0.0001; black and gray circles in Fig. 4a),

and zircons with lower common lead abundances tend to be distributed close to the concordia curve. Zircons plotted on the concordia curve and including a low common Pb concentration (red circles in Fig. 4a) exhibit two age clusters around 2860 Ma and 2910 Ma. The Th/U ratios of the orthogneiss zircons range from 0.05 to 0.72, but most have values ranging from 0.1 to 0.5.

4.3. Granite zircon U-Pb age

All zircon grains from the granite contain significant amounts of common Pb ($^{204}Pb/^{206}Pb > 0.007$; Table 3). The $^{207}Pb/^{206}Pb$ ages of zircons show a wide range from 2347 to 4593 Ma. In the Tera-Wasserburg diagram, all zircons are plotted off the concordia curve, but are distributed along two trends (Fig. 4b). The first trend is shaped by 16 zircon grains intersecting the $^{207}Pb/^{206}Pb$ axis ($^{238}U/^{206}Pb = 0$) at *ca.* 1.1 Ga and the concordia curve at *ca.* 2.1 Ga (orange line in Fig. 4b). The second trend, which is formed by four zircon grains, has a steep gradient and intersects the concordia curve at *ca.* 2.0 Ga (purple line in Fig. 4b). There is no systematic difference between the above two zircon groups under CL observation; they form apparent regression lines in the $^{204}Pb/^{206}Pb$–$^{207}Pb/^{206}Pb$ diagram (Fig. 5). The Th/U ratios of zircons vary from 0.22 to 3.08, independently of their common Pb abundance.

5. Discussion

5.1. Protolith age of the orthogneisses

CL observations indicate that most zircons from the orthogneiss show zoning from the core to rim and do not exhibit highly luminescent margins, as seen in metamorphic zircons (Fig. 3a). Most zircons have Th/U ratios of 0.1–0.5 (Table 3), which is consistent with a magmatic origin (Williams et al., 1996; Rubatto and Gebauer, 2000), rather than a metamorphic origin, as suggested by Williams and Claesson (1987). Due to the pre-ablation process during the analyses, we succeeded in analyzing the non-metamictized parts in some zircons. This enabled us to obtain some data plotted on the Tera-Wasserburg concordia curve with low common Pb abundance (Fig. 4a), although most analyses indicate a certain level of ^{204}Pb (Table 3). The data on the concordia curve show two age populations at *ca.* 2860 Ma and 2910 Ma. There is no systematic difference between zircons in these two populations under CL observation. Because of the scattered distribution pattern in the concordia diagram, we cannot identify a discordia line.

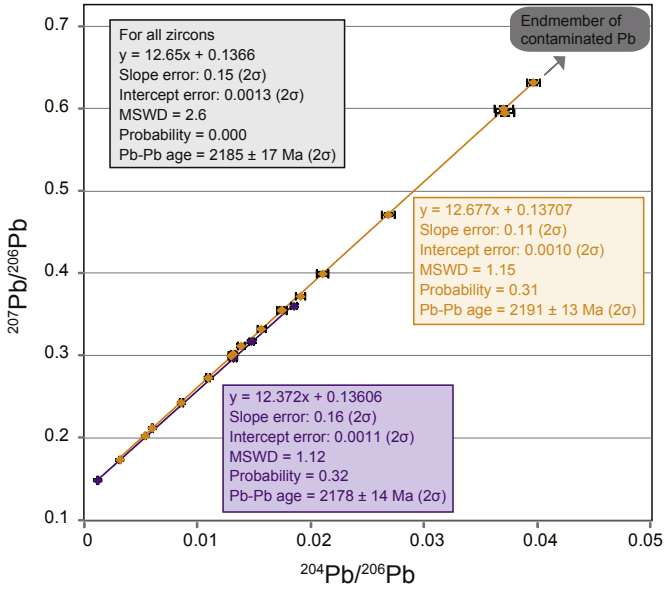

Figure 5. Isotopic crossplot showing $^{204}Pb/^{206}Pb$ vs. $^{207}Pb/^{206}Pb$ for zircons from a granite (NG12). Colors of analytical data are based on the distribution pattern in Fig. 4b. Gradients and *y*-intercepts ($^{207}Pb/^{206}Pb$-axis) of fitted lines are also shown in black (for all 20 grains), orange (for 16 grains), and purple (for 4 grains). Regression lines for each group are illustrated using the ISOPLOT program of Ludwig (2003).

Previously, the Rb-Sr isochron method applied on the granitoids near Koulamoutou and Chaillu yielded the ages of 2888 ± 40 Ma, 2765 ± 39 Ma, and 2637 ± 33 Ma (Fig. 1a; Caen-Vachette et al., 1988). The 2888 ± 40 Ma age is comparable to the age obtained from the U-Pb analyses in the present study, whereas the latter two ages (2765 ± 39 Ma and 2637 ± 33 Ma) are clearly younger than the ones obtained here. In view of the CL observations of the zircons together with the Rb-Sr isochron ages, the protolith age of the orthogneiss in East Gabonian block ranges from 2860 to 2910 Ma. Based on a previous chronological report (Caen-Vachette et al., 1988), a coeval age was reported from diorites in the Nounah-Ivindo area. Epizonal metamorphism and later magmatism in the Chaillu area at 2700–2600 Ma (Caen-Vachette et al., 1988) did not appear to influence the zircon U-Pb isotope system in the East Gabonian block.

5.2. Intrusion age of granite (N'goutou complex)

The individual $^{207}Pb/^{206}Pb$ ages are considered meaningless due to the high abundances of common lead in all zircon grains (Table 3). In the Tera-Wasserburg diagram, a regression line formed by 16 zircon grains intersects the $^{207}Pb/^{206}Pb$ axis ($^{238}U/^{206}Pb = 0$) at *ca.* 1.1 Ga and the concordia curve at around 2.1 Ga (orange line in Fig. 4b). In addition, another regression line shows a gradient steeper than that of the orange line and intersects the concordia curve at *ca.* 2.0 Ga (purple line in Fig. 4b). It is likely that these distribution patterns reflect a mixing between igneous (radiogenic) and contaminated (unradiogenic) end members. Based on the evolution model of the Pb isotopic composition in the crust by previous studies (Stacey and Kramers, 1975; Gancarz and Wasserburg, 1977; Allégre et al., 1995), the $^{207}Pb/^{206}Pb$ ratio in crust had been *ca.* 1.0 before *ca.* 2.0 Ga. Therefore, we suggest that common-lead-contaminated zircons before 2.0 Ga, or in an extreme case, the common lead was primarily involved in zircon crystallization, as commonly observed in zircons from syenite (e.g., Peng et al., 2008; Krasnobaev et al., 2011). The experimental study by Watson et al. (1997) indicated that significant amounts of Pb can be incorporated into zircons grown from a melt with high P abundance. Low phosphorus contents in studied granitoids (Table 2),

Table 2
Major element compositions of the rocks analyzed in this study by XRF.

	NG12	NG18
	Granite	Syenite
SiO_2	76.52	61.04
TiO_2	0.26	0.95
Al_2O_3	12.64	13.47
Fe_2O_3	0.54	10.48
MnO	BDL	0.46
MgO	0.01	0.12
CaO	0.08	2.00
Na_2O	0.61	5.13
K_2O	8.64	4.11
P_2O_5	BDL	0.04
Total	99.29	97.79
K_2O/Na_2O[a]	9.33	0.53
ASI[b]	1.20	0.82

BDL, below detection limit; [a] This value means molar ratio; [b] ASI, aluminum saturation index; major elements are in wt.%.

Table 3
LA-ICP-MS U-Pb isotopic analytical data for zircons from granite (NG12) and gneiss.

	$^{207}Pb/^{235}U$	Error	$^{206}Pb/^{238}U$	Error	$^{207}Pb/^{206}Pb$	Error	$^{204}Pb/^{206}Pb$	Error	$^{207}Pb/^{235}U$ age (Ma)	Error	$^{206}Pb/^{238}U$ age (Ma)	Error	$^{207}Pb/^{206}Pb$ age (Ma)	Error	Th/U
NG12 12	12.451	0.309	0.422	0.010	0.214	0.001	0.00595	0.00007	2639	24	2270	47	2936	7	0.71
NG12 16	24.471	0.607	0.495	0.012	0.358	0.002	0.01741	0.00019	3287	24	2593	52	3743	7	0.22
NG12 25	18.760	0.206	0.375	0.004	0.363	0.002	0.01850	0.00025	3030	11	2052	17	3762	8	0.55
NG12 27	16.162	0.178	0.366	0.004	0.320	0.002	0.01473	0.00021	2886	11	2012	17	3570	8	3.08
NG12 28	16.681	0.184	0.439	0.004	0.275	0.001	0.01091	0.00016	2917	11	2348	19	3337	8	1.45
NG12 29	7.466	0.082	0.361	0.003	0.150	0.001	0.00113	0.00002	2169	10	1986	16	2347	9	0.54
NG12 30	9.630	0.106	0.398	0.004	0.175	0.001	0.00311	0.00005	2400	10	2161	18	2610	9	0.36
NG12 32	70.282	0.771	0.801	0.008	0.636	0.003	0.03959	0.00054	4332	11	3794	28	4593	8	0.46
NG12 33	19.650	0.216	0.468	0.004	0.304	0.002	0.01311	0.00018	3074	11	2475	20	3493	8	0.66
NG12 35	11.441	0.126	0.406	0.004	0.205	0.001	0.00533	0.00008	2560	10	2194	18	2863	9	0.71
NG12 36	14.727	0.162	0.436	0.004	0.245	0.001	0.00851	0.00012	2798	11	2332	19	3153	8	0.80
NG12 40	39.292	0.799	0.600	0.012	0.475	0.002	0.02678	0.00061	3753	20	3032	48	4164	8	0.97
NG12 41	62.832	1.278	0.754	0.015	0.604	0.003	0.03695	0.00084	4220	21	3624	55	4518	7	0.86
NG12 42	61.025	1.241	0.739	0.015	0.599	0.003	0.03707	0.00084	4191	21	3567	54	4505	7	0.87
NG12 43	20.209	0.411	0.466	0.009	0.314	0.002	0.01381	0.00032	3101	20	2466	40	3543	8	0.23
NG12 44	28.636	0.583	0.516	0.010	0.402	0.002	0.02099	0.00048	3441	20	2683	43	3918	8	0.18
NG12 45	15.454	0.315	0.375	0.007	0.299	0.002	0.01313	0.00030	2844	20	2051	35	3466	8	1.88
NG12 47	24.373	0.496	0.494	0.010	0.358	0.002	0.01737	0.00040	3283	20	2590	42	3739	8	0.25
NG12 48	18.478	0.376	0.443	0.009	0.302	0.002	0.01293	0.00030	3015	20	2365	39	3482	8	1.61
NG12 49	21.250	0.432	0.460	0.009	0.335	0.002	0.01558	0.00036	3150	20	2439	40	3641	8	1.27
Gneiss 01	15.559	0.265	0.553	0.009	0.204	0.001	0.00002	0.00000	2850	16	2836	37	2860	8	0.57
Gneiss 02	15.757	0.268	0.560	0.009	0.204	0.001	0.00002	0.00000	2862	16	2866	38	2859	8	0.56
Gneiss 03	15.461	0.263	0.547	0.009	0.205	0.001	0.00001	0.00000	2844	16	2812	37	2867	8	0.37
Gneiss 04	15.275	0.260	0.545	0.009	0.203	0.001	0.00020	0.00001	2833	16	2806	37	2851	8	0.39
Gneiss 05	14.081	0.240	0.502	0.008	0.203	0.001	0.00097	0.00001	2755	16	2623	35	2853	8	0.21
Gneiss 06	16.589	0.282	0.573	0.009	0.210	0.001	0.00002	0.00000	2911	16	2918	38	2907	8	0.44
Gneiss 07	15.410	0.262	0.541	0.009	0.207	0.001	0.00017	0.00000	2841	16	2786	37	2880	8	0.30
Gneiss 08	14.502	0.247	0.505	0.008	0.208	0.001	0.00009	0.00000	2783	16	2634	35	2893	8	0.37
Gneiss 09	11.636	0.198	0.428	0.007	0.197	0.001	0.00052	0.00001	2576	16	2295	31	2805	8	0.10
Gneiss 10	16.610	0.283	0.572	0.009	0.210	0.001	0.00005	0.00000	2913	16	2918	38	2909	8	0.13
Gneiss 11	9.612	0.164	0.352	0.006	0.198	0.001	0.00104	0.00001	2398	16	1945	27	2810	8	0.25
Gneiss 12	15.068	0.256	0.519	0.008	0.211	0.001	0.00019	0.00000	2820	16	2693	36	2911	8	0.69
Gneiss 13	15.957	0.271	0.561	0.009	0.206	0.001	0.00006	0.00000	2874	16	2869	38	2878	8	0.30
Gneiss 14	4.185	0.078	0.187	0.003	0.163	0.000	0.00107	0.00001	1671	15	1103	19	2483	4	0.35
Gneiss 15	16.446	0.305	0.567	0.010	0.210	0.001	0.00003	0.00000	2903	18	2895	43	2909	4	0.37
Gneiss 16	15.070	0.279	0.526	0.010	0.208	0.001	0.00014	0.00000	2820	18	2726	41	2888	4	0.23
Gneiss 18	14.736	0.273	0.520	0.010	0.206	0.001	0.00017	0.00001	2798	18	2699	41	2870	4	0.26
Gneiss 19	6.155	0.114	0.255	0.005	0.175	0.000	0.00081	0.00001	1998	16	1463	24	2608	4	0.08
Gneiss 20	10.804	0.200	0.384	0.007	0.204	0.001	0.00078	0.00001	2506	17	2096	33	2858	4	0.12
Gneiss 21	12.283	0.228	0.441	0.008	0.202	0.001	0.00029	0.00001	2626	18	2354	36	2843	4	0.18
Gneiss 22	15.649	0.290	0.556	0.010	0.204	0.001	0.00002	0.00000	2856	18	2849	42	2861	4	0.48
Gneiss 23	13.397	0.248	0.470	0.009	0.207	0.001	0.00026	0.00001	2708	18	2486	38	2879	4	0.72
Gneiss 24	10.289	0.191	0.364	0.007	0.205	0.001	0.00058	0.00001	2461	17	2000	32	2868	4	0.24
Gneiss 25	16.585	0.308	0.574	0.011	0.210	0.001	0.00003	0.00000	2911	18	2923	43	2903	4	0.17
Gneiss 26	16.228	0.301	0.565	0.010	0.208	0.001	0.00003	0.00000	2890	18	2887	43	2893	4	0.25
Gneiss 27	12.924	0.199	0.456	0.007	0.205	0.001	0.00064	0.00001	2674	15	2423	30	2870	6	0.20
Gneiss 28	16.568	0.255	0.576	0.009	0.209	0.001	0.00003	0.00000	2910	15	2932	35	2895	6	0.32
Gneiss 29	16.276	0.251	0.559	0.008	0.211	0.001	0.00002	0.00000	2893	15	2863	35	2914	6	0.20
Gneiss 30	14.875	0.229	0.525	0.008	0.205	0.001	0.00024	0.00001	2807	15	2722	33	2869	6	0.25
Gneiss 31	15.034	0.232	0.511	0.008	0.213	0.001	0.00053	0.00001	2817	15	2660	33	2932	6	0.29
Gneiss 32	12.646	0.195	0.466	0.007	0.197	0.001	0.00011	0.00000	2654	15	2466	31	2800	6	0.26
Gneiss 33	14.488	0.223	0.503	0.008	0.209	0.001	0.00024	0.00001	2782	15	2629	32	2895	6	0.22
Gneiss 34	16.640	0.257	0.582	0.009	0.207	0.001	0.00006	0.00000	2914	15	2959	36	2884	6	0.25
Gneiss 35	12.846	0.198	0.449	0.007	0.207	0.001	0.00040	0.00001	2668	15	2392	30	2885	6	0.12
Gneiss 36	14.079	0.217	0.494	0.007	0.207	0.001	0.00018	0.00001	2755	15	2587	32	2880	6	0.40
Gneiss 37	11.917	0.184	0.421	0.006	0.205	0.001	0.00042	0.00001	2598	15	2265	29	2869	6	0.10
Gneiss 38	15.922	0.245	0.548	0.008	0.211	0.001	0.00018	0.00001	2872	15	2815	34	2913	6	0.37
Gneiss 39	16.544	0.255	0.567	0.008	0.212	0.001	0.00006	0.00000	2909	15	2894	35	2919	6	0.21
Gneiss 40	12.140	0.207	0.413	0.007	0.213	0.001	0.00161	0.00002	2615	16	2229	32	2930	4	0.19
Gneiss 41	14.475	0.247	0.504	0.008	0.208	0.001	0.00028	0.00001	2781	16	2631	36	2893	4	0.35
Gneiss 42	6.958	0.119	0.237	0.004	0.213	0.001	0.00343	0.00003	2106	15	1369	21	2931	4	0.11
Gneiss 43	13.249	0.226	0.460	0.008	0.209	0.001	0.00046	0.00001	2698	16	2439	34	2898	4	0.12
Gneiss 44	15.780	0.269	0.553	0.009	0.207	0.001	0.00015	0.00000	2864	16	2840	39	2880	4	0.24
Gneiss 45	10.956	0.187	0.392	0.007	0.203	0.001	0.00051	0.00001	2519	16	2131	31	2849	4	0.23
Gneiss 46	12.598	0.215	0.450	0.008	0.203	0.001	0.00026	0.00001	2650	16	2396	34	2850	4	0.22
Gneiss 47	13.048	0.222	0.468	0.008	0.202	0.001	0.00010	0.00000	2683	16	2474	35	2845	4	0.02
Gneiss 48	15.383	0.263	0.532	0.009	0.210	0.001	0.00011	0.00000	2839	16	2749	38	2904	4	0.61
Gneiss 49	15.801	0.270	0.548	0.009	0.209	0.001	0.00005	0.00000	2865	16	2817	39	2899	4	0.28
Gneiss 50	15.261	0.261	0.529	0.009	0.209	0.001	0.00027	0.00001	2832	16	2738	38	2899	4	0.27
Gneiss 51	14.791	0.252	0.519	0.009	0.207	0.001	0.00013	0.00000	2802	16	2695	37	2880	4	0.05
Gneiss 52	13.413	0.229	0.457	0.008	0.213	0.001	0.00076	0.00001	2709	16	2426	34	2928	4	0.17
Gneiss 53	7.789	0.121	0.285	0.004	0.198	0.000	0.00108	0.00001	2207	14	1616	22	2812	2	0.29
Gneiss 54	14.431	0.223	0.386	0.006	0.271	0.000	0.00617	0.00005	2778	15	2107	28	3311	2	0.68

Table 3 (*continued*)

	$^{207}Pb/^{235}U$	Error	$^{206}Pb/^{238}U$	Error	$^{207}Pb/^{206}Pb$	Error	$^{204}Pb/^{206}Pb$	Error	$^{207}Pb/^{235}U$ age (Ma)	Error	$^{206}Pb/^{238}U$ age (Ma)	Error	$^{207}Pb/^{206}Pb$ age (Ma)	Error	Th/U
Gneiss 55	14.208	0.220	0.496	0.008	0.208	0.000	0.00038	0.00001	2764	15	2597	33	2888	2	0.28
Gneiss 56	16.118	0.249	0.557	0.009	0.210	0.000	0.00003	0.00000	2884	15	2852	36	2906	2	0.31
Gneiss 57	16.308	0.252	0.558	0.009	0.212	0.000	0.00019	0.00001	2895	15	2859	36	2920	2	0.23
Gneiss 58	10.608	0.164	0.386	0.006	0.199	0.000	0.00069	0.00001	2489	14	2103	28	2821	2	0.20
Gneiss 59	11.374	0.176	0.407	0.006	0.202	0.000	0.00044	0.00001	2554	15	2203	29	2846	2	0.14
Gneiss 60	14.925	0.231	0.528	0.008	0.205	0.000	0.00004	0.00000	2810	15	2733	34	2866	2	0.18
Gneiss 61	13.597	0.210	0.485	0.007	0.204	0.000	0.00008	0.00000	2722	15	2547	33	2855	2	0.12
Gneiss 62	11.853	0.183	0.402	0.006	0.214	0.000	0.00161	0.00002	2593	15	2176	29	2937	2	0.06
Gneiss 63	14.692	0.228	0.497	0.008	0.214	0.000	0.00062	0.00001	2796	15	2600	33	2940	2	0.38

Note: all errors are quoted at 2s level.

however, are inconsistent with this interpretation. In another case, tetravalent lead can substitute zirconium site in zircon. The syenite used in this study includes ilmenite (Fig. 2a–f). Thus, the oxygen fugacity of the parent magma was not high, as lead is oxidized to tetravalent. The whole-rock chemical compositions of some syenites from the N'goutou complex indicate high Pb abundances up to 132 ppm (Moussavou and Edou-Minko, 2006). It is generally suggested that most A-type granites formed from relatively high-temperature magmas (Clemens et al., 1986; Whalen et al., 1987). The Pb diffusion rate in zircon increases with temperature (e.g., Cherniak and Watson, 2003). Therefore, high common-lead abundances in zircons are possibly attributed to Pb diffusion at a high temperature of the parent magma.

The reason for the erroneous value of the purple line on the $^{207}Pb/^{206}Pb$ axis (Fig. 4b) can be attributed to the differences in the mechanical strength and crystal structure of zircons, which could have led to an error in the correction of U/Pb ratios during the LA-ICP-MS analysis. The analyses plotted on the purple line may have been largely influenced by metamictization; however, no significant difference between the analyses of the purple and orange groups under CL observation can be seen (Fig. 3b). The U/Pb ratios shown on the orange line were also potentially affected by metamictization in varying degrees, as shown by the low accuracy of the fitting line (MSWD = 5.6; Fig. 4b). Therefore, we use lead isotopes to facilitate discussions about obtaining a more accurate igneous age.

In order to estimate the apparent radiogenic $^{207}Pb/^{206}Pb$ value, we plotted the data on a crossplot of $^{204}Pb/^{206}Pb$ vs. $^{207}Pb/^{206}Pb$ (Fig. 5). In analogy with Fig. 4b, two trends are clearly recognizable, both showing high linearity ($r^2 > 0.9997$). In these mixing lines, the values on the $^{207}Pb/^{206}Pb$ axis represent radiogenic Pb isotopic ratios, which is least affected by the unradiogenic component. One regression line intersects the $^{207}Pb/^{206}Pb$ axis at 0.13707 ± 0.0010 (orange line) and another at 0.13606 ± 0.0011 (purple line). The former corresponds to the $^{207}Pb/^{206}Pb$ age of 2191 ± 13 Ma (MSWD = 1.15) and the latter is equivalent to the $^{207}Pb/^{206}Pb$ age of 2178 ± 14 Ma (MSWD = 1.12), based on the ISOPLOT program of Ludwig (2003). Apart from a few data, Th/U ratios in most zircons are within the range of representative igneous zircons (Table 3; Williams et al., 1996; Rubatto and Gebauer, 2000). We prefer the age of 2191 ± 13 Ma (orange line) as the granite igneous age because zircon data yielding 2178 ± 14 Ma contain an erroneous value at the $^{207}Pb/^{206}Pb$ axis in the Tera-Wasserburg diagram (purple line in Fig. 4b).

The igneous age obtained in this study is greater than that estimated from the upper intercept in the U-Pb concordia diagram (2027 ± 55 Ma; Moussavou and Edou-Minko, 2006), but falls within that estimated from the Rb-Sr isochron (2143 ± 143 Ma; Bonhomme et al., 1982) due to its large error. In addition to the volume of analytical data, because common lead was not evaluated by Moussavou and Edou-Minko (2006), 2191 ± 13 Ma is considered a more accurate igneous age for the granite.

5.3. Implications

The N'goutou complex, including the syenite and granite, intrudes into the FA and FB units in the Francevillian Group (Fig. 1b). Therefore, the ages of the two units could be greater than 2191 ± 13 Ma. This improves the correlations of the Francevillian Group with sedimentary sequences in other areas (Fig. 6). The largest manganese ore (Hotazel Formation) in Earth's history was deposited just after the last Paleoproterozoic Snowball Earth event (after *ca.* 2.22 Ga; Cornell et al., 1996; Bekker et al., 2010; Bekker and Holland, 2012), and is possibly contemporary with the manganese-rich carbonate rocks in the FB unit. Above the manganese deposits, the FB unit consists of macroscopic structures interpreted as colonial organisms and microbial/algal consortia (Albani et al., 2010; Moussavou et al., 2015). The appearance of these organisms was older than previously proposed and likely dates back to the aftermath of the last Paleoproterozoic Snowball Earth event. These large-sized organisms might have evolved in concert with the oxidation of the atmosphere-ocean system after the Snowball Earth event. The deposition of black shales in the FB-FC units was previously considered concurrent with a worldwide deposition of organic carbon-rich black shales (Shunga event; Melezhik et al., 1999) between 2.05 and 1.9 Ga (Gauthier-Lafaye, 2006). However, the newly obtained igneous age for the N'goutou complex does not support this idea, but indicates that the deposition of FB unit likely preceded the Shunga event. The organic

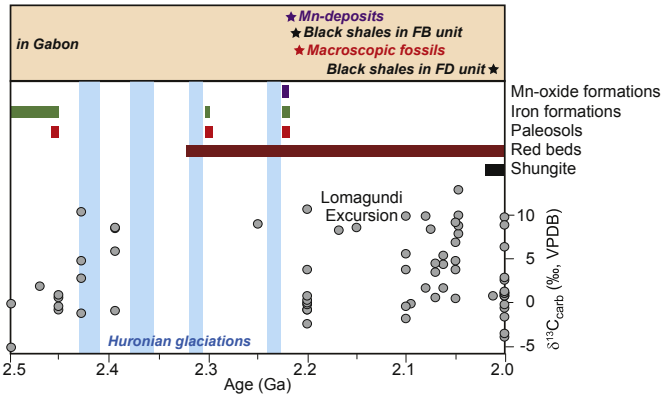

Figure 6. Redox indicators of the ancient atmosphere-ocean system (modified from Rye and Holland, 1998; Melezhik et al., 1999; Bekker et al., 2006, 2010; Pierrehumbert et al., 2011; Bekker and Holland, 2012) and secular carbon-isotope variations in the early Paleoproterozoic seawater (modified from Bekker and Kaufman, 2007).

carbon-rich black shales of the FD unit are more suitable as sediments during the Shunga event than the FB unit. This correlation is further supported by the chemostratigraphic study wherein a negative carbon isotope excursion in the FD unit was associated with so-called shungite deposits in Fennoscandia (Canfield et al., 2013).

6. Conclusions

(1) The protolith ages of orthogneiss in the East Gabonian block range from 2860 Ma to 2910 Ma. Epizonal metamorphism and later magmatism at 2700–2600 Ma did not influence the U-Pb isotopic composition of zircons in the orthogneiss.
(2) The lead isotopic variation in zircons from the granite can be explained by the mixing of two components, with an igneous age of 2191 ± 13 Ma. This age constrains the minimum depositional age of the FA and FB units in the Francevillian Group.
(3) The deposition of manganese-rich carbonate rocks, organic carbon-rich black shales, and the emergence of the macroscopic organisms in the FB unit in Gabon Republic occurred just after the last Paleoproterozoic Snowball Earth event, before *ca.* 2.2 Ga.

Acknowledgements

This work was partly supported by a grant for “Chronostratigraphy for the Mesoproterozoic strata in Jixian, North China (No. 26800259)” and “Hadean BioScience (No. 26106002)” from the Ministry of Education, Culture, Sports, Science, and Technology, Japan. We thank the reviewer for the comments and appreciate Prof. M Santosh for the editorial handling.

References

Albani, A.E.L., Bengtson, S., Canfield, D.E., Bekker, A., Macchiarelli, R., Mazurier, A., Hammarlund, E.U., Boulvais, P., Dupuy, J.-J., Fontaine, C., Fürsich, F.T., Gauthier-Lafaye, F., Janvier, P., Javaux, E., Ossa, F.O., Pierson-Wickmann, A.-C., Riboulleau, A., Sardini, P., Vachard, D., Whitehouse, M., Meunier, A., 2010. Large colonial organisms with coordinated growth in oxygenated environments 2.1 Gyr ago. Nature 466, 100–104.
Allegre, C.J., Manhes, G., Göpel, C., 1995. The age of the Earth. Geochimica et Cosmochimica Acta 59, 1445–1456.
Amard, B., Bertrand-Sarfati, J., 1997. Microfossils in 2000 Ma old cherty stromatolites of the Franceville Group, Gabon. Precambrian Research 81, 197–221.
Bekker, A., Holland, H.D., 2012. Oxygen overshoot and recovery during the early Paleoproterozoic. Earth and Planetary Science Letters 317, 295–304.
Bekker, A., Karhu, J.A., Kaufman, A.J., 2006. Carbon isotope record for the onset of the Lomagundi carbon isotope excursion in the Great Lakes area, North America. Precambrian Research 148, 145–180.
Bekker, A., Kaufman, A.J., 2007. Oxidative forcing of global climate change: a biogeochemical record across the oldest Paleoproterozoic ice age in North America. Earth and Planetary Science Letters 258, 486–499.
Bekker, A., Slack, J.F., Planavsky, N., Krapež, B., Hofmann, A., Konhauser, K.O., Rouxel, O.J., 2010. Iron formation: the sedimentary product of a complex interplay among mantle, tectonic, oceanic, and biospheric processes. Economic Geology 105, 467–508.
Bonhomme, M.G., Gauthier-Lafaye, F., Weber, F., 1982. An example of Lower Proterozoic sediments: the Francevillian in Gabon. Precambrian Research 18, 87–102.
Bros, R., Stille, P., Gauthier-Lafaye, F., Weber, F., Clauer, N., 1992. Sm-Nd isotopic dating of Proterozoic clay material: an example from the Francevillian sedimentary series, Gabon. Earth and Planetary Science Letters 113, 207–218.
Caen-Vachette, M., Vialette, Y., Bassot, J.P., Vidal, P., 1988. Apport de la géochronologie isotopique à la connaissance de la géologie gabonaise. Chronique de la Recherche Minière 491, 35–53 (in French).
Canfield, D.E., Ngombi-Pemba, L., Hammarlund, E.U., Bengtson, S., Chaussidon, M., Gauthier-Lafaye, F., Meunier, A., Riboulleau, A., Rollion-Bard, C., Rouxel, O., Asael, D., Pierson-Wickmann, A.-C., Albani, A.E.L., 2013. Oxygen dynamics in the aftermath of the Great Oxidation of Earth's atmosphere. Proceedings of the National Academy of Sciences 110, 16736–16741.
Cherniak, D.J., Watson, E.B., 2003. Diffusion in zircon. Reviews in Mineralogy and Geochemistry 53, 113–143.
Clemens, J.D., Holloway, J.R., White, A.J.R., 1986. Origin of an A-type granite: experimental constraints. American Mineralogist 71, 317–324.
Cornell, D.H., Schütte, S.S., Eglington, B.L., 1996. The Ongeluk basaltic andesite formation in Griqualand West, South Africa: submarine alteration in a 2222 Ma Proterozoic sea. Precambrian Research 79, 101–123.
Dutkiewicz, A., George, S.C., Mossman, D.J., Ridley, J., Volk, H., 2007. Oil and its biomarkers associated with the Palaeoproterozoic Oklo natural fission reactors, Gabon. Chemical Geology 244, 130–154.
Eggins, S.M., Kinsley, L.P.J., Shelley, J.M.G., 1998. Deposition and element fractionation processes during atmospheric pressure laser sampling for analysis by ICP-MS. Applied Surface Science 127, 278–286.
Gancarz, A.J., 1978. U-Pb age (2.05×10^9 years) of the Oklo uranium deposit. In: Proceedings of the Natural Fission Reactors, IAEA Symposium Proceedings, Vienna, pp. 513–520.
Gancarz, A.J., Wasserburg, G.J., 1977. Initial Pb of the Amitsoq gneiss, west Greenland, and implications for the age of the Earth. Geochimica et Cosmochimica Acta 41, 1283–1301.
Gauthier-Lafaye, F., 2006. Time constraint for the occurrence of uranium deposits and natural nuclear fission reactors in the Paleoproterozoic Franceville Basin (Gabon). Geological Society of America Memoirs 198, 157–167.
Gauthier-Lafaye, F., Weber, F., 2003. Natural nuclear fission reactors: time constraints for occurrence, and their relation to uranium and manganese deposits and to the evolution of the atmosphere. Precambrian Research 120, 81–100.
Gauthier-Lafaye, F., Weber, F., Ohmoto, H., 1989. Natural fission reactors of Oklo. Economic Geology 84, 2286–2295.
Günther, D., Heinrich, C.A., 1999. Enhanced sensitivity in laser ablation-ICP mass spectrometry using helium-argon mixtures as aerosol carrier. Journal of Analytical Atomic Spectrometry 14, 1363–1368.
Han, T.M., Runnegar, B., 1992. Megascopic eukaryotic algae from the 2.1-billion-year-old Negaunee Iron-Formation, Michigan. Science 257, 232–235.
Higashino, F., Kawakami, T., Tsuchiya, N., Satish-Kumar, M., Ishikawa, M., Grantham, G.H., Sakata, S., Hattori, K., Hirata, T., 2015. Geochemical behavior of zirconium during Cl-rich fluid or melt infiltration under upper amphibolite facies metamorphism—a case study from Brattnipene, Sør Rondane Mountains, East Antarctica. Journal of Mineralogical and Petrological Sciences 110, 166–178.
Holland, H.D., 1999. When did the Earth's atmosphere become oxic? A reply. The Geochemical News 100, 20–22.
Holland, H.D., 2005. 100th anniversary special paper: sedimentary mineral deposits and the evolution of earth's near-surface environments. Economic Geology 100, 1489–1509.
Holliger, P., 1988. Ages U-Pb définis in situ sur oxydes d'uranium à l'analyseur ionique: méthodologie et conséquences géochimiques. In: Comptes rendus de l'Académie des sciences. Série 2, Mécanique, Physique, Chimie, Sciences de l'univers, Sciences de la Terre, vol. 307, pp. 367–373 (in French).
Horie, K., Hidaka, H., Gauthier-Lafaye, F., 2005. U-Pb geochronology and geochemistry of zircon from the Franceville series at Bidoudouma, Gabon. Geochimica et Cosmochimica Acta 69, A11.
Jackson, S.E., Pearson, W.L., Griffin, W.L., Belousova, E.A., 2004. The application of laser ablation-inductively coupled plasma-mass spectrometry to in situ U-Pb zircon geochronology. Chemical Geology 211, 47–69.
Jaffey, A.H., Flynn, K.F., Glendenin, L.E., Bentley, W.T., Essling, A.M., 1971. Precision measurement of half-lives and specific activities of ^{235}U and ^{238}U. Physical Review C 4, 1889–1906.
Jochum, K.P., Brueckner, S.M., 2008. Reference materials in geoanalytical and environmental research – review for 2006 and 2007. Geostandards and Geoanalytical Research 32, 405–452.
Kopp, R.E., Kirschvink, J.L., Hilburn, I.A., Nash, C.Z., 2005. The Paleoproterozoic snowball Earth: a climate disaster triggered by the evolution of oxygenic photosynthesis. Proceedings of the National Academy of Sciences of the United States of America 102, 11131–11136.
Krasnobaev, A.A., Popov, V.S., Belyatskii, B.V., 2011. Zirconology of nepheline syenite of the Berdyaush Massif (southern urals). Doklady Earth Sciences 436, 134–137.
Ludwig, K.R., 2003. User's Manual for Isoplot 3.00: a Geochronological Toolkit for Microsoft Excel (No. 4).
Machida, S., Ishii, T., Kimura, J.-I., Awaji, S., Kato, Y., 2008. Petrology and geochemistry of cross-chains in the Izu-Bonin back arc: three mantle components with contributions of hydrous liquids from a deeply subducted slab. Geochemistry, Geophysics, Geosystems 9 (5), Q05002. http://dx.doi.org/10.1029/2007GC001641.
Melezhik, V.A., Fallick, A.E., Filippov, M.M., Larsen, O., 1999. Karelian shungite—an indication of 2.0-Ga-old metamorphosed oil-shale and generation of petroleum: geology, lithology and geochemistry. Earth-Science Reviews 47, 1–40.
Moussavou, M., Edou-Minko, A., 2006. Contribution a l'histoire thermo-tectonique precambrienne du complexe annulaire de N'goutou par la geochimie et lageochronologie U/Pb sur mineraux accessoires (Bassin Francevillien d'Okondja, Gabon). Africa Geoscience Review 13, 53–61.
Moussavou, M., Edou-Minko, A., Mbina Mounguengui, M., Ortega, R., Fleury, G., Roudeau, S., Carmona, A., Genty, D., Blamart, D., Tchikoundzi, C., Makaya, M., Musavu Moussavou, B., Ndong Ondo, S., Ogandaga Agondjo, M., Dewilde, F., Delorme, G., de Parseval, Ph., Weil, R., Maire, R., 2015. Multicellular consortia preserved in biogenic ductile-plastic nodules of Okondja Basin (Gabon) by 2.1 Ga. Journal of Geology and Geosciences 4, 195. http://dx.doi.org/10.4172/2329-6755.1000195.
Nagy, B., 1993. Kerogens and Bitumens in Precambrian Uraniferous Ore Deposits: Witwatersrand, South Africa, Elliot Lake, Canada, and the Natural Fission Reactors, Oklo, Gabon. In: Bitumens in Ore Deposits. Springer, Berlin Heidelberg, pp. 287–333.

Nagy, B., Gauthier-Lafaye, F., Holliger, P., Mossman, D.J., Leventhal, J.S., Rigali, M.J., 1993. Role of organic matter in the Proterozoic Oklo natural fission reactors, Gabon, Africa. Geology 21, 655–658.

Naudet, R., 1991. Oklo: des re'acteurs nucle'aires fossiles. Collection du Commissariat á l'Energie Atomique, Paris, p. 695.

Neuilly, M., Bussac, J., Frejacques, C., Nief, G., Vendryes, G., Yvon, J., 1972. Sur l'existence dans un passé reculé d'une réaction en chaîne naturelle de fissions, dans le gisement d'uranium d'Oklo (Gabon). Comptes Rendus de l'Académie des Sciences Paris 275, 1847–1849 (in French).

Peng, P., Zhai, M., Guo, J., Zhang, H., Zhang, Y., 2008. Petrogenesis of triassic post-collisional syenite plutons in the Sino-Korean Craton: an example from North Korea. Geological Magazine 145, 637–647.

Pierrehumbert, R.T., Abbot, D.S., Voigt, A., Koll, D., 2011. Climate of the Neoproterozoic. Annual Review of Earth and Planetary Sciences 39, 417.

Préat, A., Bouton, P., Thiéblemont, D., Prian, J.P., Ndounze, S.S., Delpomdor, F., 2011. Paleoproterozoic high $\delta^{13}C$ dolomites from the Lastoursville and Franceville basins (SE Gabon): stratigraphic and synsedimentary subsidence implications. Precambrian Research 189, 212–228.

Rubatto, D., Gebauer, D., 2000. Use of Cathodoluminescence for U-pb Zircon Dating by Ion Microprobe: Some Examples from the Western Alps. In: Cathodoluminescence in Geosciences. Springer, Berlin Heidelberg, pp. 373–400.

Ruffenach, J.C., 1978. Etude des migrations de l'uranium et des terres rares sur une carotte de sondage et application a' la de'termination de la date des re'actions nicle'aires. In: Proceedings of the Natural Fission Reactors, IAEA Symposium Proceedings, Vienna, pp. 441–471 (in French).

Rye, R., Holland, H.D., 1998. Paleosols and the evolution of atmospheric oxygen: a critical review. American Journal of Science 298, 621–672.

Sakata, S., Hattori, K., Iwano, H., Yokoyama, T.D., Danhara, T., Hirata, T., 2014. Determination of U-Pb ages for young zircons using a laser ablation-ICP-mass spectrometry coupled with attenuator ion detection device. Geostandards and Geoanalytical Research 38, 409–420.

Sláma, J., Košler, J., Condon, D.J., Crowley, J.L., Gerdes, A., Hanchar, J.M., Horstwood, M.S.A., Morris, G.A., Nasdala, L., Norberg, N., Schaltegger, U., Schoene, B., Tubrett, M.N., Whitehouse, M.J., 2008. Plešovice zircon — a new natural reference material for U-Pb and Hf isotopic microanalysis. Chemical Geology 249, 1–35.

Stacey, J.S., Kramers, J.D., 1975. Approximation of terrestrial lead isotope evolution by a two-stage model. Earth and Planetary Science Letters 26, 207–221.

Thiéblemont, D., Bouton, P., Préat, A., Goujou, J.C., Tegyey, M., Weber, F., Obiang, M.E., Joron, L.L., Treuil, M., 2014. Transition from alkaline to calc-alkaline volcanism during evolution of the Paleoproterozoic Francevillian basin of eastern Gabon (Western Central Africa). Journal of African Earth Sciences 99, 215–227.

Tunheng, A., Hirata, T., 2004. Development of signal smoothing device for precise elemental analysis using laser ablation-ICP-mass spectrometry. Journal of Analytical Atomic Spectrometry 19, 932–934.

Watson, E.B., Chemiak, D.J., Hanchar, J.M., Harrison, T.M., Wark, D.A., 1997. The incorporation of Pb into zircon. Chemical Geology 141, 19–31.

Weber, F., 1968. Une serie precambrienne du Gabon: le Francevillien. Sedimentologie, geochimie, relations avec les gites mineraux associes. In: Memoires du Service de la Carte Geologique d'Alsace-Lorraine 28. Strasbourg, 328 pp.

Whalen, J.B., Currie, K.L., Chappell, B.W., 1987. A-type granites: geochemical characteristics, discrimination and petrogenesis. Contributions to Mineralogy and Petrology 95, 407–419.

Wiedenbeck, M., Alle, P., Corfu, F., Griffin, W.L., Meier, M., Oberli, F., van Quadt, A., Roddick, J.C., Spiegel, W., 1995. Three natural zircon standards for U-Th-Pb, Lu-Hf, trace element and REE analyses. Geostandards Newsletter 19, 1–23.

Williams, I.S., Buick, I.S., Cartwright, I., 1996. An extended episode of early Mesoproterozoic metamorphic fluid flow in the Reynolds Range, central Australia. Journal of Metamorphic Geology 14, 29–47.

Williams, I.S., Claesson, S., 1987. Isotopic evidence for the Precambrian provenance and Caledonian metamorphism of high-grade paragneisses from the Seve Nappes, Scaninavian Caledonides: II. Ion microprobe zircon U-Th-Pb. Contributions to Mineralogy and Petrology 97, 205–217.